JOURNAL OF MATERIALS SCIENCE 12 (1977) 1338–1348

The failure processes, morphology and mechanical properties of a co-polyimide glass based on benzophenone tetracarboxylic acid dianhydride

ROGER J. MORGAN, JAMES E. O'NEAL
McDonnell Douglas Research Laboratories, McDonnell Douglas Corporation, St. Louis, Missouri, USA

The phyiscal structure, failure processes and mechanical properties of solution-soluble co-polyimide films based on benzophenone tetracarboxylic acid dianhydride are reported as a function of sample preparation. The failure processes and mechanical response are modified by the presence of residual solvent and microvoids, which are produced by the elimination of solvent clusters from the glass. The polyimide is amorphous, with the exception of a few isolated clusters of poorly formed spherulites and networks of 50 to 500 nm wide lamellae. The deformation modes observed when thin films were strained directly in the electron microscope were crazing, shear-band deformation and an edge-yielding phenomena. Edge-yielding, which has characteristics of both crazing and shear-banding, occurred in ~ 1 μm wide bands which were 20 to 30° to the tensile stress direction. Shear-band deformation occurred in fine ~ 100 nm wide bands, which exhibited a sharp boundary between themselves and their surroundings. TEM indicated that the shear strain was uniform within these bands. Microvoids, 1.5 to 15 nm diameter, were found to initiate shear bands some of which were ~ 1 nm wide. These bands increased in width by tearing at the microvoid initiation sites.

1. Introduction

Aromatic heterocyclic polymers generally have good flame resistance and the ability to withstand high temperatures. Polyimides are the most widely used of the heterocyclic aromatic group of polymers. Their uses include adhesives, coatings, matrices for composite materials, fibres, electrical insulators, bearings and seals. The utilization of polyimides is, however, somewhat limited by their intractable nature which causes fabrication difficulties.

Polyimides are generally prepared by a two-stage procedure [1-12]. The first stage involves the reaction of a primary diamide with a tetrabasic acid anhydride to form the polyamic acid. Ring closure (imidization) occurs in the second stage by polycondensation with the elimination of water. Koton [8] and Laius *et al.* [9] have concluded that during imidization, the rate of cyclization diminishes because of a decrease in polymer chain mobility. They further point out the need for high-temperature treatments (> 200° C) to achieve a high cyclization efficiency in the solid state. More recently, Sacher and Sedor [10] noted that complete cyclization is not likely. The presence of uncyclized "amic acid" groups in the polymer chain enhances chain flexibility but deteriorates thermal stability [8], and also allows water to degrade the polymer by selective hydrolysis at the "amic acid" sites [13].

A few studies on the structure-failure-process mechanical-property relations of polyimides have been reported. A number of workers have investi-

© 1977 Chapman and Hall Ltd. Printed in Great Britain.

gated the glassy-state, molecular motion of polyimides in relation to their structure by dielectric loss and dynamic mechanical measurements [14–27]. However, there are many inconsistencies in the published data, possibly because of different concentrations of unreacted species in the glasses investigated. The morphological structures of polyimide fibres and oriented and non-oriented films have been studied by a number of workers by X-ray diffraction and electron microscopy [2, 7, 8, 18, 26, 28–31]. Spherulitic, fibrillar, globular and lamellae structures were reported. The physical structure depends on polymerization conditions, thermal history, solubility parameter of the solvent, film thickness and fabrication stresses. Koton [8] has considered the effect of chemical structure on the mechanical response of polyimides. There have been no attempts, as yet, to elucidate the failure processes of polyimides.

In this paper we investigate the physical structure, failure processes and mechanical properties of a solution-soluble co-polyimide based on benzophenone tetracarboxylic acid dianhydride (Upjohn, Polyimide 2080). This solution-soluble polyimide was chosen because (a) according to the manufacturer, the polymer is fully imidized and (b) thin films can be cast from solution for electron microscope studies. The tensile mechanical properties, fracture topographies, morphology and failure processes of the polyimide are reported as a function of sample preparation conditions. Bright-field TEM was utilized to monitor the morphology and failure processes. For the failure process studies, films were strained directly in the electron microscope. The presence of solvent clusters in the polyimide films was monitored by dielectric loss measurements.

2. Experimental

2.1. Materials and sample preparation

The solution-soluble co-polyimide based on benzophenone tetracarboxylic acid dianhydride (Upjohn, Polyimide 2080) used in this study is a random co-polyimide, which is designated here as BTAD-polyimide. It consists of approximately 80% recurring units with the structure

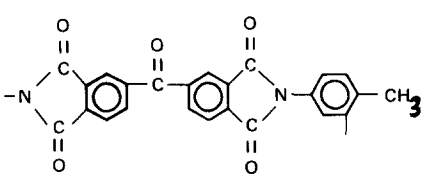

and approximately 20% recurring units with the structure [32]

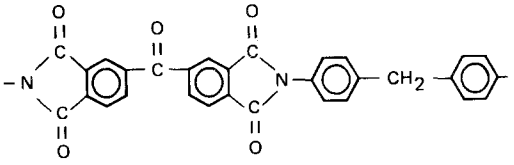

The polymer, a fully imidized and polymerized polyimide, was initially in a solution of *N*-methyl-2-pyrollidone.

For the mechanical property studies, polymer films (~ 0.1 mm thick) were cast from the as-received *N*-methyl-pyrollidone-polyimide solution on glass plates and then transferred to fresh plates after annealing for 2 h at 50° C in a vacuum. These films were then heated in vacuum for 24 h at temperatures from 75 to 320° C and subsequently cooled to room temperature at 2° C min^{-1}. Dogbone-shaped specimens with a 3.0 cm gauge length and a width of 0.35 cm within the gauge length were punched from the films by suitably shaped dies.

Films, ~ 1 μm thick, suitable for straining directly in the electron microscope, were cast on glass plates from a 10% solution of the polyimide in *N*-methyl-pyrollidone (Eastman, purity met infrared transparency specifications). Thinner, ~ 100 nm thick, films for morphological studies in the electron microscope were prepared from a 1% solution of the polyimide. Both sets of films were annealed at 50° C for 24 h in vacuum and then floated on to water and picked up with fresh glass slides. The films were subsequently step-annealed under vacuum at 110, 150, 200, 240 and 320° C for 24 h at each temperature. This series of increasing annealing temperatures ensures that the films do not strongly adhere to the glass slides, and hence, minimizes fabrication stresses in the films.

For dielectric loss studies, 0.1 mm thick films of BTAD-polyimide and polystrene (Monsanto, research grade) were cast from *N*-methyl-pyrollidone. Discs, 2.5 cm diameter and suitable for dielectric loss measurements, were punched from these sheets.

2.2. Experiment

The room temperature tensile mechanical properties of the polyimide films were measured with a table model tensile tester (Instron TM-S-1130) at a cross-head speed of 0.5 cm min^{-1}. Dielectric loss measurements were made at 100 Hz from 100 to

250 K utilizing an automatic dielectrometer (Tetrahedron, Audrey II). The low-temperature dielectric cell was similar to that developed by McCammon and Work [33]. The fracture topographies were monitored by an optical microscope (Zeiss Ultraphot II). Bright-field TEM was used to investigate the morphology of the ~ 100 nm thick polyimide films. The failure processes of BTAD-polyimide were monitored by straining ~ 1 μm thick films directly in the electron microscope (JEOL model JEM100B), at a strain rate of ~ 10^{-2} min^{-1}, using an EM-SEH specimen elongation holder. Rectangular specimens were adhered to standard cartridge specimen holders with Duco cement (E.I. duPont). The specimen was introduced into the microscope by installing the elongation holder in the side-entry goniometer of the microscope.

3. Results and discussion

3.1. Mechanical properties and fracture topographies

The effect of 24 h of anneal temperature from 77 to 320° C on the tensile strength, ultimate elongation and Young's modulus of BTAD-polyimide is shown in Fig. 1. The wt % of *N*-methyl-pyrollidone remaining in the polyimide after each anneal temperature is shown in Table I.

TABLE I 24 h anneal temperature versus wt % N-methyl-pyrollidone in BTAD-polyimide

Sample no.	Anneal temperature (°C)	wt % N-methyl-pyrollidone
A-1	77	18
A-2	135	10
A-3	193	5
A-4	247	1
A-5	300	0.1
A-6	320	0.01

The polyimide glass containing 18 wt % of solvent (A-1, Table I) exhibited a lower tensile strength and modulus and a greater ultimate elongation than glasses annealed at higher temperatures and containing less solvent. The primary mode of deformation of this glass was microscopic shear-band deformation because of the overall plasticizing effect of the solvent. Fracture occurred by rapid crack propagation through the oriented neck. The fracture topography characteristic of this mode of failure [34] is illustrated in the optical micrograph in Fig. 2a. The parallel markings in the fracture surface result from segments of the

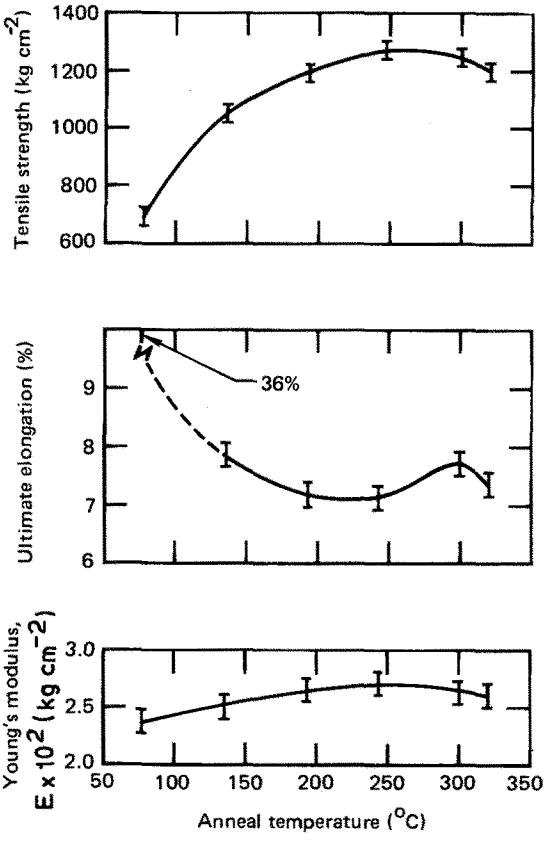

Figure 1 The room-temperature tensile strength, ultimate elongation and Young's modulus of BTAD-polyimide versus 24 h anneal temperature under vacuum.

crack running on different but parallel planes. At higher magnifications, this fracture surface was found to consist of a series of microvoids which probably arise from the original presence of solvent clusters in the glass.

Evidence that solvent clusters exist in the polyimide is found from dielectric loss measurements. In Fig. 3 a plot of dielectric loss (100 Hz) versus temperature from 100 to 250 K reveals a loss peak near 180 K for the BTAD-polyimide-*N*-methyl-pyrollidone system. The intensity of the loss peak decreases with decreasing solvent content. A loss peak also occurs near 170 K when *N*-methyl-pyrollidone is present in polystyrene (Fig. 3). In the absence of absorbed solvent, BTAD-polyimide and polystyrene do not exhibit these loss peaks. These observations suggest that the loss peaks are characteristic of the solvent rather than the host polymer and are attributed to the T_g of solvent clusters [35]. The loss peak is still present for the polyimide glass containing 7.7 wt % solvent, which

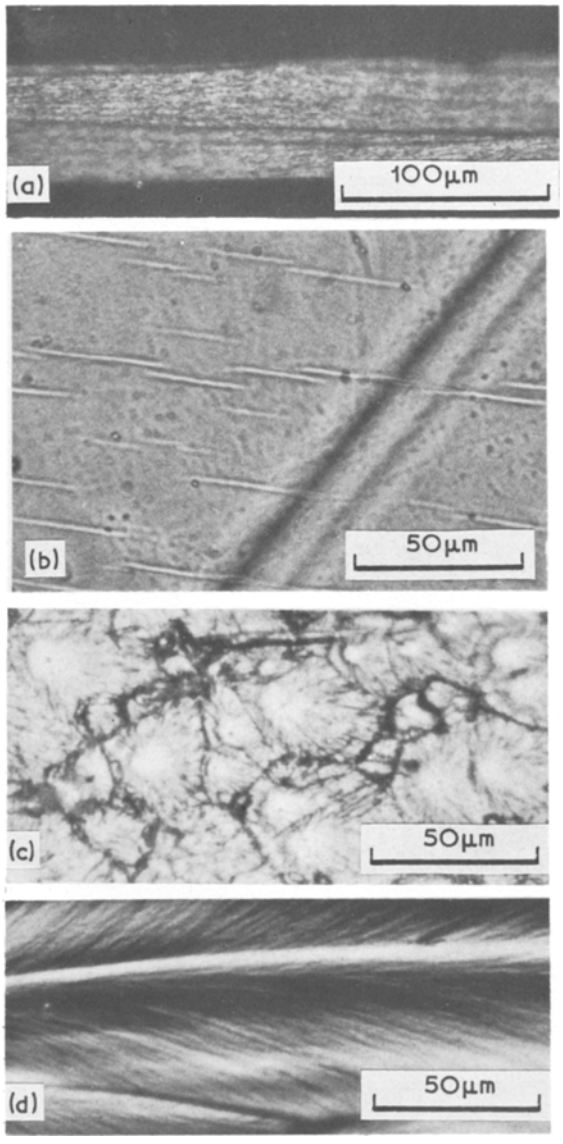

Figure 2 Optical micrographs of (a) fracture topography of BTAD-polyimide, 24 h anneal-77° C, (b) crazes and shear band in transmission of BTAD-polyimide, 24 h anneal-135° C, (c) fracture topography of BTAD-polyimide, 24 h anneal-193° C and (d) fracture topography of BTAD-polyimide, 24 h anneal-300° C.

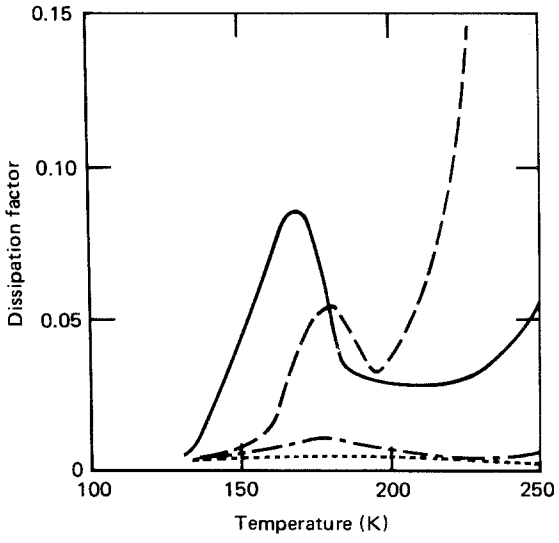

Figure 3 Dielectric dissipation factor (100 Hz) versus temperature for (a) BTAD-polyimide-*N*-methyl-pyrollidone system containing (i) 47.7 wt % (- - -), (ii) 19.8 wt % (— • —) and (iii) 7.7 wt % (. . . . .) of solvent and (b) polystyrene-*N*-methyl-pyrollidone system (——) containing 15.4 wt % of solvent.

suggests that solvent clusters exist in glasses annealed for 24 h at $\gtrsim$ 135° C (see Table I).

For annealing temperatures from 77 to 300° C, BTAD-polyimide becomes harder, as indicated by increases in tensile strength and modulus and decreases in ultimate elongation, with increasing temperature and decreasing solvent content (Fig. 1 and Table I). In this annealing temperature range, BTAD-polyimide exhibited both shear-band deformation and crazing, with the latter being the predominant mode of deformation and the cause of failure. The transmission optical micrograph in Fig. 2b illustrates both the presence of crazes and shear-band deformation in a fractured BTAD-polyimide glass that was annealed at 135° C for 24 h.

The fracture topography of the polyimide glasses annealed from 77 to 300° C illustrates that failure occurs by a crazing process. For example, the optical micrograph in Fig. 2c shows that the fracture topography of BTAD-polyimide, which was annealed at 193° C for 24 h, consists of a series of impinging crazes. Each craze is characterized in the fracture topography by a region consisting of a small, dark central region surrounded by a smooth, mirror-like region and an outer region with radial river markings. The dark central region is associated with a craze initiation cavity [36]. From studies primarily on polystyrene and epoxy glasses, the initial stages of void growth and coalescence within a craze involve fracture through the centre of the craze [37–39]. The smooth region surrounding the initiation cavity is associated with slow crack growth through the median of the craze with subsequent relaxation of the craze remnants [36, 40–44]. The size of the mirror-like region varies with temperature, molecular weight and strain rate

[45–48]. The river markings are steps formed by the subdivision of the main crack into segments running on different but parallel planes. This subdivision results from the interaction of the crack front with the craze structure [39]. The large number of craze initiation sites in the polyimide glasses is associated with the presence of either solvent clusters, which would enhance craze initiation and propagation, and/or microvoids, produced by evaporation of solvent clusters, which act as stress concentrators. The softer mechanical response of the glasses with higher solvent concentrations is associated with the solvent-enhancing craze initiation and propagation.

Annealing at $\gtrsim 300^\circ$ C ($T_g \simeq 310^\circ$ C) eliminates the microvoids and/or any remaining solvent clusters. This results in a markedly different fracture topography, as illustrated in the optical micrograph in Fig. 2d. The river markings and their direction on the fracture surface suggest that failure occurred by propagation of a craze initiating at the specimen edge. After annealing $\gtrsim 300^\circ$ C (A-5, A-6, Table I), the polyimide glasses exhibit a softening trend relative to the glass annealed at 247° C, as indicated by slightly lower tensile strengths and higher ultimate elongations (Fig. 1). This phenomenon, if real, may be caused by the different configurational arrangements and packing of the polymer chains formed from the polymer melt rather than from a polymer-solvent melt.

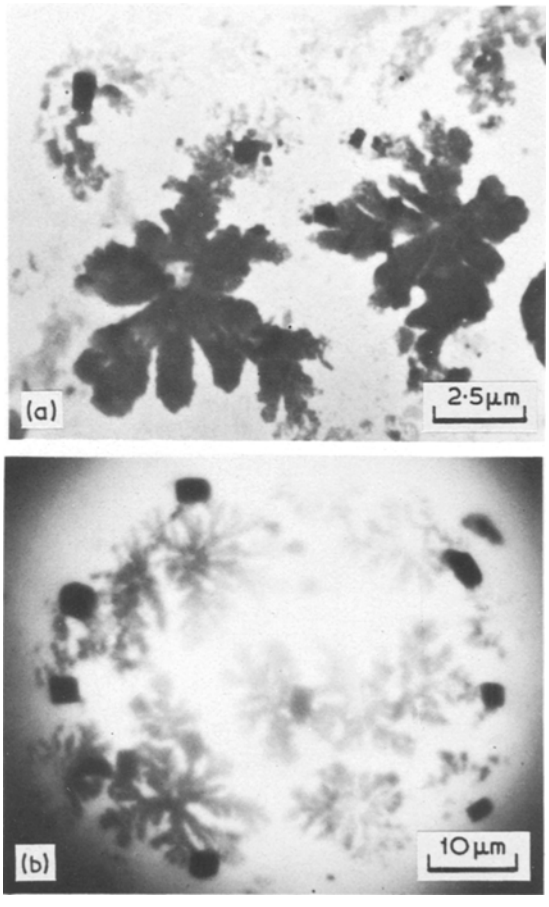

Figure 4 (a) and (b) Bright-field TEMs illustrating isolated islands of spherulitic and lamellae crystalline structures in BTAD-polyimide.

3.2. Morphology

The morphology of ~100 nm thick BTAD-polyimide films was investigated by bright-field TEM. Only isolated islands of crystalline entities were observed in these films. The bright-field TEMs in Fig. 4a and b show clusters of poorly formed spherulites. The spherulites are up to 20 μm diameter with 0.3 to 2 μm wide radial arms. Lamellae with a maximum width of 3.5 μm are particularly evident at the ends of the spherulitic arms (Fig. 4b). In Fig. 4a, networks of interconnected 50 to 500 nm wide lamellae are also evident. At higher magnifications, 10 nm wide square- and irregularly-shaped lamellae were observed in these films. The melting point (T_m) of the more highly ordered crystalline lamellae should be ~600° C, assuming $T_g/T_m \simeq 2/3$ [49]. Thermal degradation of the polyimide, however, will occur prior to the melting of these crystals.

Stresses are produced during the fabrication of the ~100 nm thick BTAD-polyimide films. The elimination of the *N*-methyl-pyrollidone solvent from the film causes shrinkage of the BTAD-polyimide film. If, however, the polymer strongly adheres to the glass slide, stresses will develop from (a) the inability of the polymer to shrink and (b) the disparity of the coefficients of expansion of the polyimide film and inorganic glass substrate. To minimize such stresses, the polyimide films were floated on to water after annealing at 50° C for 24 h in vacuum, and then picked up on a fresh slide. Generally, the films did not strongly adhere to the fresh slide during the subsequent annealing at higher temperatures (> 100° C) and could easily be separated from the slide after annealing. If, however, the films were not transferred to a fresh slide, they strongly adhered to the glass slide after annealing above 100° C. Such films could only be removed from the slide by etching with a ~10 wt % aqueous NaOH solution. Films prepared by the latter procedure (i.e. annealed on glass slides

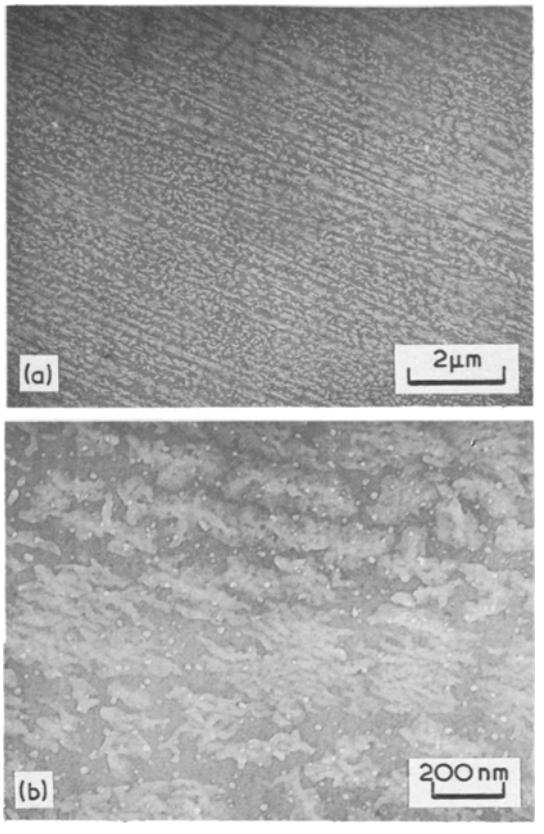

Figure 5 (a) and (b) Bright-field TEMs of parallel, long-range irregularities in film thickness from relaxation of fabrication stresses in BTAD-polyimide.

at and above 275° C) exhibited parallel, long-range irregularities in thickness which were revealed by bright-field TEM (Fig. 5a and b). We suggest that this phenomenon results from the relaxation of fabrication stresses which occur by local yielding and causes subsequent thinning of the film. This relaxation process occurs only near T_g (i.e. $\gtrsim$ 275° C) where the yield stress is sufficiently low. Such a phenomenon is not observed in films annealed below 275° C.

3.3. Failure processes

The failure processes of BTAD-polyimide were studied by straining ~ 1 μm thick films directly in the electron microscope at a strain-rate of ~ 10^{-2} min^{-1}. The predominant mode of deformation in these films was crazing, however deformation also occurred by shear-banding and edge-yielding. The polyimide films were deformed in the electron microscope at an order of magnitude lower strain-rate than that employed in the mechanical property studies with the 1 mm thick films. The following evidence suggests that shear-band deformation is favoured at the lower strain-rates employed for straining films in the electron microscope. The strain-rate dependence of the shear yield stress of polycarbonate has been reported to be greater than that of the crazing stress [34]. In addition, the temperature dependence of the shear yield stress, which follows the same trend as the strain-rate dependence, has been reported to be greater than that of the temperature dependence of the crazing stress for other polymer glasses [50, 51]. Hence, at lower strain-rates, shear yielding becomes more favourable relative to crazing.

The BTAD-polyimide films strained in the microscope failed by crack propagation through pre-existing crazes. In the ~ 1 μm thick films, the crack propagated through the median of the craze or along the craze–matrix boundary interface, as seen in the bright-field TEMs of fractured crazes in Fig. 6a and b respectively. Fractured fibrils, 30 to 80 nm diameter, are evident as dark circular regions in these micrographs. For thinner, ~ 100 nm thick films, crazing occurred by a thinning of the polymer at the craze tip. The bright-field TEM in Fig. 7a shows thin, ~ 40 nm diameter circular regions (which appear light in the micrograph) separated by dark, thicker 4 to 6 nm diameter fibrils. Further from the craze tip, the crack propagates through the thinned polymer film. Structures < 2 nm, which appear as dark regions in the micrograph, are discernable in the thin regions within the craze. The TEM in Fig. 7b illustrates the presence of a network of oriented polymer chains in thin regions within a fractured craze. This latter observation suggests that polymer segments rather than larger

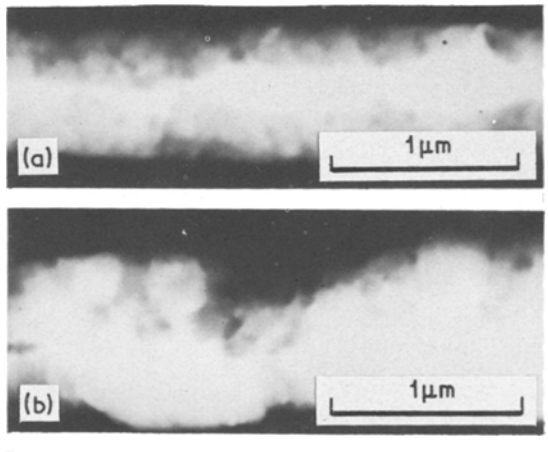

Figure 6 Bright-field transmission electron micrographs of craze remnants in BTAD-polyimide after crack propagation (a) through the craze median and (b) along the craze-matrix boundary interface.

morphological entities are involved in the flow processes that occur during craze-growth in this polymer.

Edge-yielding occurred in a number of the BTAD-polyimide films that were strained in the electron microscope. These films became progressively thinner along their edges with increasing strain. The bright-field TEM in Fig. 8 shows the thinned regions, which appear light in the micrograph, along the specimen edge. The thinning occurs as $\sim 1\,\mu m$ wide bands which propagate from the specimen edge at an angle of 20 to 30° to the tensile stress direction. Dark regions of undeformed material, $\lesssim 1\,\mu m$ diameter, are distributed throughout the thinned region of the film and are shown more clearly at higher magnifications in Fig. 9. These regions appear dark in the micrographs because they are thicker and probably more ordered than the surrounding material. Such undeformed regions are possibly precrystalline regions which only become clearly evident in the micrographs during this deformation process. The deformable polymer separates from these regions primarily along the edge parallel to the longitudinal growth direction of the thinned bands. Deformation within the thinned bands occurs perpendicular to their longitudinal growth direction, as shown by the presence of fibrils in this direction in Fig. 10. The edge-yielding phenomenon has some characteristics of both crazing and shear-banding. The direction of the local, complex deformation processes relative to the applied tension in this yielding phenomenon depends on the local anisotropy of the deformed material and the presence of the undeformed regions. Beardmore and Rabinowitz [52], in recent studies on crazing in anisotropic polymers, have shown that craze growth occurs in directions governed by the principal strain rather than being orthogonal to the principal tensile stress. Harris and Ward [53], in earlier studies on oriented poly (ethylene terephthalate), reported "shear crazes" whose planes are at ~ 50° to the tensile axis.

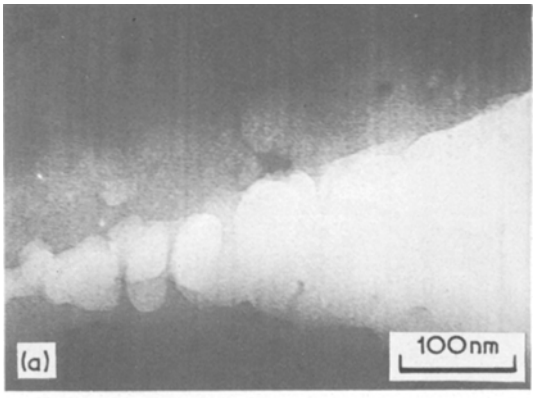

Figure 7 (a) and (b) Bright-field TEMs of craze structure in ~ 100 nm thick BTAD-polyimide film.

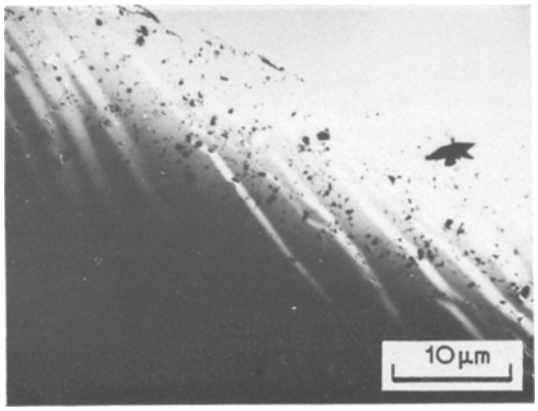

Figure 8 Bright-field TEM of edge-yielding phenomenon in BTAD-polyimide film.

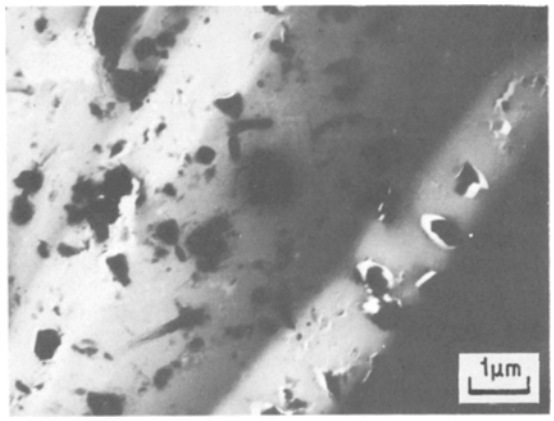

Figure 9 Bright-field TEM of dark regions of undeformed material in the region where edge-yielding has occurred in BTAD-polyimide.

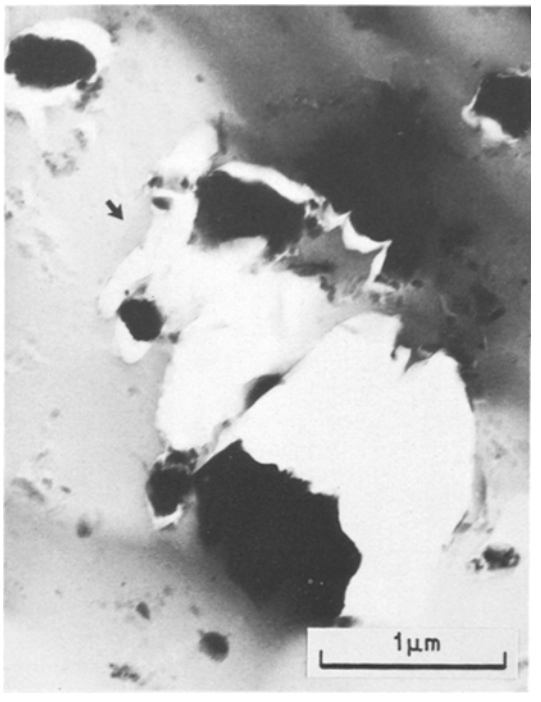

Figure 10 Bright-field TEM illustrating fibrils within an edge-yield band. (Arrow indicates longitudinal growth direction of yield band.)

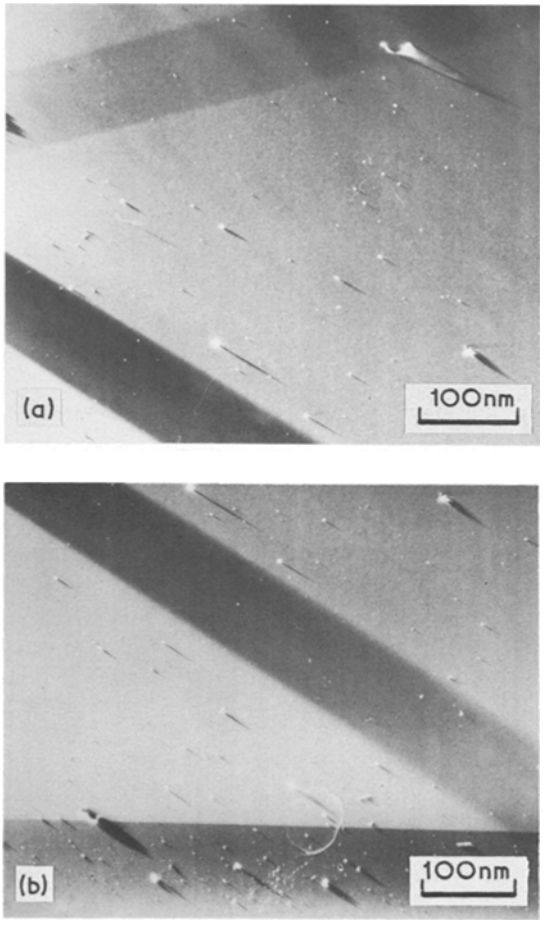

Figure 11 (a) and (b) Bright-field TEMs of shear-band propagation in BTAD-polyimide.

Shear-band deformation also occurred in the BTAD-polyimide films when they were strained in the electron microscope. Rather than diffuse shear-band zones, isolated ~ 100 nm wide microscopic shear bands were observed. Such bands are illustrated in the bright-field TEMs in Fig. 11a and b. The shear bands appear as dark bands in the micrograph which is indicative of denser packing of the polymer chains as a result of molecular flow and orientation. Wu and Li [54] have characterized two shear-band deformation processes in polystyrene; one appears as fine shear bands and the other as diffuse shear zones. We observed only the fine shear bands on deformation of BTAD-polyimide in the electron microscope. These bands exhibited a constant width with an extremely sharp boundary with the surrounding material. We examined numerous bright-field TEMs of these shear bands and found no evidence of any contrast differences within the bands. This observation suggests that the shear strain is uniform within these bands. Brady and Yeh [55, 56] reported a nodular structure within shear bands, and Wu and Li [54] claim that the shear strain is nonuniform and greater in the centre of the shear bands.

Microvoids of 1 to 15 nm diameter, which appear white in the micrographs, are evident in Fig. 11a and b and are shown at higher magnifications in Fig. 12a and b. These microvoids act as stress-concentration sites on a molecular level and initiate shear bands, some of which are ~ 1 nm wide, as indicated by the dark bands originating from the microvoids in Fig. 12a and b. The remarkable resolution and contrast of these micrographs, we believe, results from the film collecting a charge and electrons accumulating on the top surface of the film. The original presence of solvent clusters during film preparation, detected by dielectric loss studies, and their subsequent elimination from the glass could be responsible for many of the microvoids observed in these micrographs.

There is a general trend towards longer shear bands with increasing microvoid diameters as shown from the plot in Fig. 13. From examination

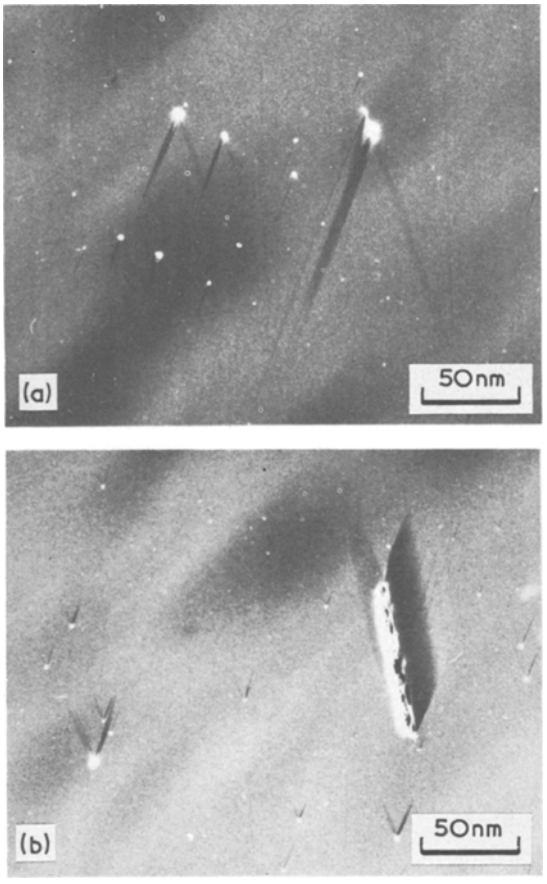

Figure 12 (a) and (b) Bright-field TEMs of microvoid shear-band initiation sites and associated shear bands in BTAD-polyimide.

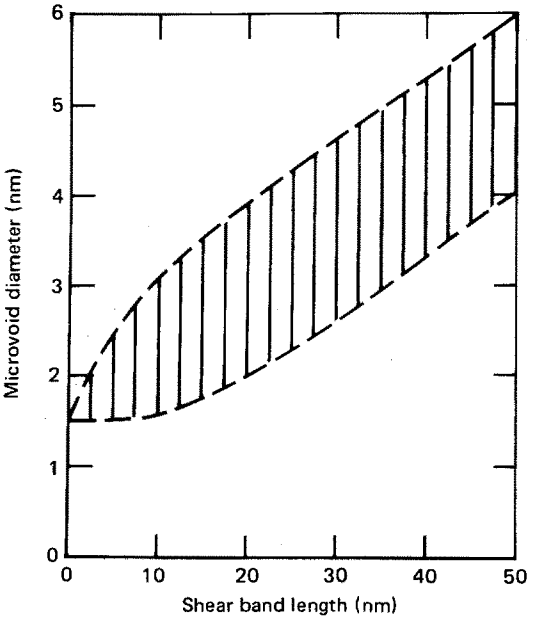

Figure 13 Plot of diameter of microvoid shear-band initiation site versus shear-band length.

of a number of micrographs, ~90% of the data fell within the shaded area shown in Fig. 13. Microvoids $\lesssim 1.5$ nm diameter did not initiate shear bands that were detectable in the micrographs. The scatter in the data in Fig. 13 arises from the modification of the shear-band length by the proximity of other microvoids and the ~100 nm wide shear bands.

Microvoids $\lesssim 4$ nm diameter show signs of tearing in Fig. 12a, which could be the initial stages of the process responsible for widening the shear band. The ~90 nm wide shear band and associated initiation region in Fig. 12b may have resulted from the tearing of an initiating microvoid. The mechanism by which a shear band ceases to widen or thicken and only becomes longer may be related to unique stress-field conditions at the shear-band initiation regions.

4. Conclusions

(1) The mechanical response and failure processes of a solution-cast co-polyimide film based on benzophenone tetracarboxylic acid dianhydride (BTAD-polyimide) are affected by residual solvent content. For high solvent concentrations, $\gtrsim 15$ wt %, the primary mode of deformation is macroscopic shear-band deformation, with failure occurring by rapid crack propagation through the oriented material. For lower solvent concentrations, $\lesssim 10\%$, both shear-banding and crazing occur, with the latter being the predominant mode of deformation and the cause of failure. Solvent clusters and the microvoids produced when these clusters are eliminated from the polyimide glass act as craze initiation sites throughout the glass. Annealing at $\gtrsim 300°$ C eliminates these microvoids, and failure primarily originates from surface crazes.

(2) BTAD-polyimide exhibits little crystallinity. A few isolated clusters of poorly formed spherulites and networks of 50 to 500 nm wide lamellae were observed. Isolated 10 nm lamellae also exist throughout the glass.

(3) From BTAD-polyimide films strained directly in the electron microscope, three microscopic modes of deformation were observed: crazing, fine shear-band propagation, and an edge-yielding phenomenon. Edge-yielding, which has some of the characteristics of both crazing and shear-banding, results in a thinning of the film at the

specimen edge. This yielding phenomenon occurred in ~ 1 μm wide bands which were at an angle of 20 to 30° to the tensile stress direction. Shear-band deformation occurs in fine bands ~ 100 nm wide. These bands exhibit a sharp boundary between themselves and the surrounding undeformed material. From the lack of any contrast differences within the shear bands in bright-field TEM, we conclude that there is uniform shear strain within these bands. Shear bands, some of which were ~ 1 nm wide, were found to initiate from 1.5 to 15 nm diameter microvoids. The length of these shear bands increases with increasing microvoid diameter. The shear band width increases by a tearing of the microvoid initiation sites.

Acknowledgements

We wish to acknowledge Drs D. P. Ames and C. J. Wolf (MDRL, St. Louis) for their support and encouragement of this work. This research was conducted under the McDonnell Douglas Indepedent Research and Development Program.

References

1. G. M. BOWER and L. W. FROST, *J. Polymer Sci.* **A1** (1963) 3135.
2. C. E. SROOG, A. L. ENDREY, S. V. ABRAMO, C. E. BERR, W. M. EDWARDS, and K. L. OLIVIER, *ibid* **A3** (1965) 1373.
3. J. A. KREUZ, A. L. ENDREY, F. P. GAY and C. E. SROOG, *ibid A-1*, 4 (1966) 2607.
4. L. A. LAIUS, M. I. BESSONOV, Ye. V. KALLISTOVA, N. A. ADROVA, and F. S. FLORINSKII, *Vysokomol. soyed.* **A9** (1967) 2185.
5. E. L. JOHNSON, *J. Appl. Polymer Sci.* **15** (1971) 2825.
6. D. H. KAEBLE and E. H. CIRLIN, *J. Polym. Sci. C.* **35** (1971) 79, 101.
7. K. N. VLASOVA, M. L. DOBROKHTOVA, L. N. SUVOROVA and I. N. EMELYANOVA, *Soviet Plastics* **10** (1971) 26.
8. M. M. KOTON, *Vysokomol soyed.* **A13** (1971) 1348.
9. L. A. LAIUS, M. L. BESSONOV and F. S. FLORINSKII, *ibid* **A13** (1971) 2006.
10. E. SACHER and D. G. SEDOR, *J. Polymer Sci. (Polymer Phys. Ed.)* **12** (1974) 629.
11. R. FOUNTAIN and T. W. HAAS, *J. Appl. Polymer Sci.* **19** (1975) 1767.
12. I. Ye. KARDASH, A. Ya. ARDASHNIKOV, F. S. YAKUSHIN and A. N. PRAVEDNIKOV, *Vysokomol. soyed.* **A17** (1975) 598.
13. R. DEIASI, *J. Mater. Sci.* **10** (1975) 1951.
14. I. E. AMBORSKI, *Ind. Eng. Chem.* **2** (163) 189.
15. A. D. MAIR, M. C. SHEN and A. V. TOBOLSKY, Office Naval Res. Tech. Rept. RLT-82 (1964).
16. S. L. COOPER, A. D. MAIR and A. V. TOBOLSHY, *Textile Res. J.* **35** (1965) 1110.
17. M. BACCAREDDA, E. BUTTA, V. FROSINI and S. DePETRIS, *Mater. Sci. Eng.* **3** (1968) 157.
18. R. M. IKEDA, *Polymer Letters* **4** (1966) 353.
19. W. WRASIDLO and J. M. AUGL, *J. Polymer Sci. A-1* **7** (1969) 321.
20. G. A. BERRIER and D. E. KLINE, *J. Appl. Polymer Sci.* **12** (1968) 593.
21. E. BUTTA, S. DePETRIS and M. PASQUIRI, *ibid* **13** (1969) 1073.
22. W. WRASIDLO, *J. Macromol. Sci.-Phys. B6* **3** (1972) 559.
23. J. K. GILLHAM, K. D. HALLOCK and S. J. STADNICKI, *J. Appl. Polymer Sci.* **16** (1972) 2595.
24. J. K. GILLHAM and H. C. GILLHAM, *Polymer Eng. Sci.* **13** (1973) 447.
25. I. I. PEREPECHKO, A. MIRZAKARIMOV, V. V. RODIONOV and V. D. VOROB'EV, *Vysokomol. soyed.* **A16** (1974) 1648.
26. N. A. ADROVA, A. I. ARTYUKHOV, Yu. G. BAKLAGINA, T. I. BORISOVA, M. M. KOTON, N. V. MIKHAILOVA, V. N. NIKITIN and A. V. SIDOROVICH, *Vysokomol. soyed.* **A16** (1974) 1658.
27. M. I. BESSONOV, N. P. KUZNETSOV, N. A. ADROVA and F. S. FLORINSKII, *ibid* **A16** (1974) 2093.
28. Ye. G. LUR'E, L. G. KAZARYAN, E. L. UCHASTKINA, V. V. KOVRIGA, K. N. VLASOVA, M. L. DOBROKHOTOVA and L. N. YEMEL'YANOVA, *ibid* **A13** (1971) 603.
29. Sh. TUICHIEV, L. N. KORZHAVIN, O. Ye. PROKHOROV, B. M. GINZBURG and S. Ya. FRENKEL, *ibid* **A13** (1971) 1463.
30. L. G. KAZARYAN, D. Ya. TSVANKIN, B. M. GINZBURG, Sh. TUICHIEV, L. N. KORZHAVIN and S. Ya. FRENKEL, *ibid* **A14** (1972) 1199.
31. B. M. GINZBURG, Sh. TUICHIYEV and S. Ya. FRENKEL, *ibid* **A17** (1975) 609.
32. Upjohn Co., U.S. Patent No. 3, 708, 458 (1973).
33. R. D. McCAMMON and R. N. WORK, *Rev. Sci. Instrum.* **36** (1965) 1169.
34. R. J. MORGAN and J. E. O'NEAL, *J. Polymer Sci. (Polymer Phys. Ed.)* **14** (1976) 1053.
35. R. J. MORGAN and L. E. NIELSEN, *J. Polymer Sci. A-2*, **10** (1972) 1575.
36. J. MURRAY and D. HULL, *Polymer* **10** (1969) 451.
37. *Idem, J. Polymer Sci. A-2*, 8 (1970) 1521.
38. P. BEAHAN, M. BEVIS and D. HULL, *J. Mater. Sci.* 8 (1972) 162.
39. R. J. MORGAN and J. E. O'NEAL, *J. Mater. Sci.* (In press).
40. S. RABINOWITZ, A. R. KRAUSE and P. BEARDMORE, *J. Mater. Sci.* 8 (1973) 11.
41. M. J. DOYLE, *ibid* **10** (1975) 159.
42. *Idem, ibid* **10** (1975) 300.
43. J. HOARE and D. HULL, *ibid* **10** (1975) 1861.
44. H. EL-HAKEEM, G. P. MARSHALL, E. L. ZICHY and L. E. CULVER, *J. Appl. Polymer Sci.* **19** (1975) 3093.
45. F. ZANDEMAN, Publs. Scient. Tech. Minist. Air, Paris No. 291 (1954) Ch. IV.
46. S. B. NEWMAN and I. WOLOCK, *J. Appl. Phys.* **29** (1958) 49.
47. I. WOLOCK and S. B. NEWMAN in "Fracture Pro-

cesses in Polymeric Solids," Edited by B. Rosen (Interscience, 1964.) Chapter IIC.
48. R. J. BIRD, J. MANN, G. POGANY and G. ROONEY, *Polymer* 7, (1966) 307.
49. L. E. NIELSEN, "Mechanical Properties of Polymers and Composites," Vol. 1 (Marcel Dekker, New York, 1974).
50. S. S. STERNSTEIN and L. ONGCHIN, *Polymer Preprints* **10** (1969) 117.
51. R. N. HAWARD, B. M. MURPHY and E. F. T. WHITE, *J. Polymer Sci. A-2*, 9 (1971) 801.
52. P. BEARDMORE and S. RABINOWITZ, *J. Mater. Sci.* **10** (1975) 1763.
53. J. S. HARRIS and I. M. WARD, *ibid* **5** (1970) 573.
54. J. B. C. WU and J. C. M. LI, *ibid* **11** (1976) 434.
55. T. E. BRADY and G. S. Y. YEH, *J. Appl. Phys.* **42** (1971) 4622.
56. *Idem, J. Mater. Sci.* 8 (1973) 1083.

Received 29 October and accepted 22 November 1976.